Imaging of alkyne-functionalized ruthenium complexes for photoactivated chemotherapy

Busemann, A.

4

VISUALIZING THE INVISIBLE: IMAGING OF RUTHENIUM-BASED PACT AGENTS IN FIXED CANCER CELLS

*Two alkyne-functionalized complexes with the formula [Ru(HCC-tpy)(NN)(Hmte)]$(PF_6)_2$ were synthesized, where HCC-tpy = 4′-ethynyl-2,2′:6′,2″-terpyridine, NN = 3,3′-biisoquinoline (i-biq, [**2**]$(PF_6)_2$), or di(isoquinolin-3-yl)amine (i-Hdiqa, [**4**]$(PF_6)_2$), and Hmte = 2-(methylthio)ethanol. The geometry of the complexes is preserved after functionalization, and the alkyne moiety has no effect on the photosubstitution quantum yield ($\Phi_{[2]} = 0.022$ and $\Phi_{[4]} = 0.080$). Cellular uptake, on the other hand, was doubled after alkyne functionalization, resulting in increased cytotoxicity against A549 cancer cells for both complexes in the dark and after light activation ($EC_{50,\,light} = 5$ and 7 μM). Post-treatment fluorophore labelling via copper-catalyzed azide-alkyne cycloaddition in fixed cells showed that the complexes accumulate in the cytoplasm, and are located in the perinuclear region.*

4.1 Introduction

While the photosubstitution properties of ruthenium-based photoactivated chemotherapy (PACT) agents are studied extensively, the behavior of these newly designed complexes in the cell environment stays rather unexplored. To obtain information about the fate of a drug in a biological context, the drug distribution and its interaction with cellular targets must be studied *in cellulo*. When such studies are possible, notably when the compound is emissive, its mode of action can be more easily correlated to its efficiency and cytotoxicity profile, enabling improvement of the drug design and increasing its chances to get into the clinics.[1] However, most ruthenium-based PACT agents are non-emissive because their photoactivation mechanism is based on low-lying ^{3}MC states that quench the ^{3}MLCT-based emission and lead to photosubstitution. If the PACT drug candidate does not contain ligands with inherent fluorescence properties, such as anthraquinone and anthracene,[2, 3] the study of the cellular fate of those photoactivatable complexes is very challenging.

A common method to visualize non-emissive drugs in cells is the synthesis of drug conjugates that are covalently linked to an organic fluorophore moiety to enable microscopy imaging of the compounds. The first example for a metal-based drug, a cisplatin derivative covalently bound to an emissive carboxyfluorescein diacetate (CFDA) moiety, was reported by Molenaar *et al*.[4] They confirmed the accumulation of the platinum compound in the nucleus, as expected for cisplatin. Hereafter, many other groups investigated fluorophore-labeled drug derivatives.[5-9] However, the fluorophore moiety can drastically change the chemical properties of the original drug, which affects its cell uptake and intracellular distribution.[10] In addition, due to its size and/or charge, the fluorophore moiety might strongly modify the interaction of the drug with its target, leading to a mode of action that does not necessarily resemble that of the original drug.[11] Therefore, a new method for the visualization of non-emissive compounds was developed by Bierbach and coworkers.[11] This method is based on labelling after cell treatment and cell fixation, which allows for the preservation of the chemical and biological properties of the drug. Cellular uptake, intracellular distribution, and target interaction are not affected by the fluorophore moiety. The fluorophore can be attached in the fixed cells using different methods, *e.g.* click chemistry. So far, the groups of DeRose[12] and Che[13, 14] have picked up this method and studied the cellular distribution of their metal complexes. To be able to perform the labeling, the drug needs to be functionalized with a handle (*e.g.* an alkyne), which is a chemical group that

specifically reacts with a complementary reactive group (*e.g.* an azide) attached to the fluorophore. While the biological activity of the complex thus is not affected by the fluorophore, the effect of the handle on the drug's properties has not been discussed extensively.

In this work, the PACT agents described in Chapter 3, [Ru(tpy)(i-biq)(Hmte)]$(PF_6)_2$ [**1**]$(PF_6)_2$ and [Ru(tpy)(i-Hdiqa)(Hmte)]$(PF_6)_2$ [**3**]$(PF_6)_2$ (where tpy = 2,2′:6′,2″-terpyridine, i-biq = 3,3'-biisoquinoline, i-Hdiqa = di(isoquinolin-3-yl)amine, and Hmte = 2-(methylthio)ethanol), were functionalized with the smallest handle possible, *i.e.* a simple alkyne group, to obtain the drug analogues [**2**]$(PF_6)_2$ and [**4**]$(PF_6)_2$ ([Ru(HCC-tpy)(NN)(Hmte)]$(PF_6)_2$, where NN = i-biq or i-Hdiqa, Scheme 4.1). With these complexes in hand, we considered answering the following questions: i) does even such minimal functionalization of the PACT agent have an effect on its photochemical and biological properties? ii) Does the small handle allow for fluorophore labeling *via* click chemistry in fixed cells? And iii) if so, what is the cellular localization of the PACT agent? By doing so, non-emissive PACT agents and their light-dependent interactions are visualized for the first time in fixed cells by post-treatment labeling.

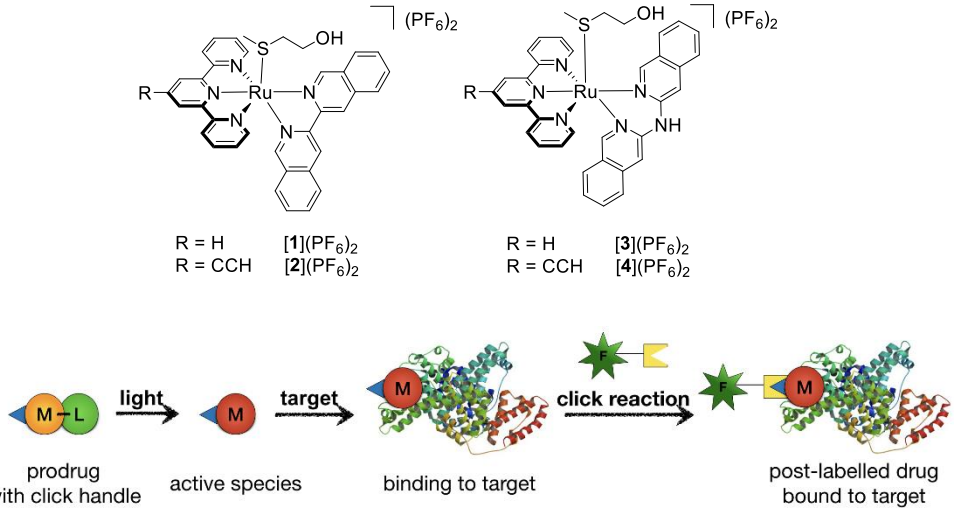

Scheme 4.1. Alkyne-functionalized PACT agents (top) for post-treatment labeling to preserve their biological activity (bottom).

4.2 Results and Discussion

4.2.1 Synthesis and Characterization

The alkyne-functionalized PACT agents [**2**](PF$_6$)$_2$ and [**4**](PF$_6$)$_2$ were synthesized following the synthetic route described in Chapter 2 for [Ru(HCC-tpy)(bpy)(Hmte)](PF$_6$)$_2$ (where bpy = 2,2′-bipyridine, Scheme AIV.1). Like for the synthesis of [Ru(HCC-tpy)(bpy)(Hmte)](PF$_6$)$_2$, the terminal alkyne was protected with a TBDMS group (TBDMS = *tert*-butyldimethylsilyl) during all synthetic steps. Such protection prevents the reaction between the terminal alkyne and the metal center, as it would result in the formation of undesired side products that are difficult to remove. After TBDMS removal with five equivalents of potassium fluoride and precipitation of the complex as its PF$_6$ salt, the products were isolated as NMR-pure solids in 62 and 83% yield, respectively. ^{1}H NMR spectra in acetone-d$_6$ showed the singlet for the free alkyne at 4.59 and 4.52 ppm for [**2**](PF$_6$)$_2$ and [**4**](PF$_6$)$_2$, respectively, demonstrating successful deprotection (Figure AIV.1 and AIV.2).

Single crystals suitable for X-ray structure determination for complex [**2**](PF$_6$)$_2$ were obtained by slow vapor diffusion of diethyl ether into a solution of the complex in cyclopentane (see Figure 4.1). Selected bond lengths and angles are summarized in Table 4.1, together with those reported for the alkyne-free complex [**1**](PF$_6$)$_2$ (Chapter 3). The terminal alkyne has a bond length (C≡C) of 1.188(7) which is similar to published data,[15] and it lies in the plane of the tpy ligand (N2-C8-C37 = 177.46°). The Ru-N bond lengths of the polypyridyl ligands tpy and i-biq are not significantly different in complexes [**2**](PF$_6$)$_2$ and [**1**](PF$_6$)$_2$. The bond length of the S-bound thioether ligand is also not affected by alkyne functionalization (Ru-S = 2.3623(10) and 2.368(3) Å for [**2**](PF$_6$)$_2$ and [**1**](PF$_6$)$_2$, respectively). Density functional theory (DFT) calculations for [**2**](PF$_6$)$_2$ are in agreement with the X-ray results. Since crystal growth for complexes [**4**](PF$_6$)$_2$ was unsuccessful, the complex structure obtained by DFT modeling was compared to that of [**3**](PF$_6$)$_2$ (Table 4.1). The comparison of the results obtained by DFT calculations showed that the structures of [**4**]$^{2+}$ and [**3**]$^{2+}$ are very similar. Overall, the addition of the alkyne moiety to the tpy ligand has no significant effect on the bond lengths or the geometry of the complexes.

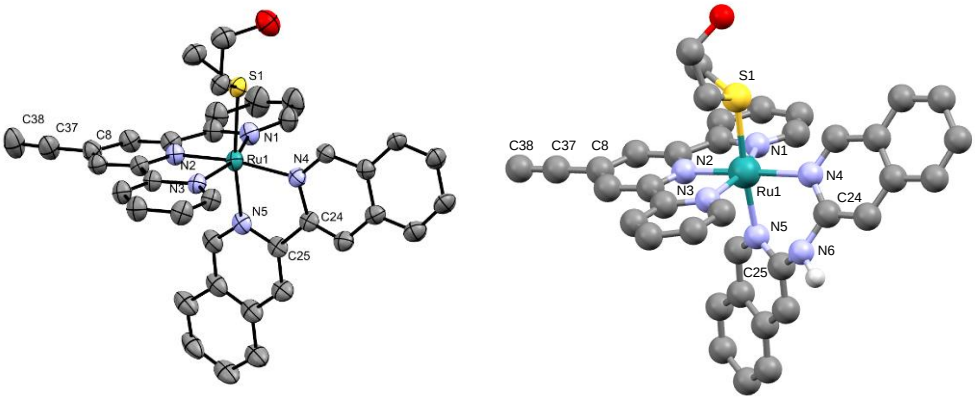

Figure 4.1. Displacement ellipsoid (50% probability level) of the cationic part as observed in the crystal structure of [**2**](PF$_6$)$_2$ (left). Disorder, counter ions, and H atoms have been omitted for clarity. DFT model of [**4**]$^{2+}$ (right).

Table 4.1. Selected bond lengths (Å) and angles (°) of [**1**](PF$_6$)$_2$, [**2**](PF$_6$)$_2$, [**3**]$^{2+}$, and [**4**]$^{2+}$.

	[**1**](PF$_6$)$_2$ [a]	[**2**](PF$_6$)$_2$	[**3**]$^{2+}$ [a,b]	[**4**]$^{2+}$ [b]
Ru-N1	2.071(9)	2.086(3)	2.095	2.098
Ru-N2	1.967(10)	1.963(3)	1.978	1.974
Ru-N3	2.073(10)	2.073(3)	2.114	2.111
Ru-N4	2.104(10)	2.093(3)	2.138	2.141
Ru-N5	2.074(9)	2.069(6)	2.115	2.112
Ru-S1	2.368(3)	2.3623(10)	2.396	2.402
C8-C37	-	1.435(6)	-	1.423
C37-C38	-	1.188(7)	-	1.202
N1-Ru1-N2	79.3(4)	79.61(13)	79.17	79.13
N2-Ru1-N3	80.1(4)	79.59(13)	78.90	79.01
N1-Ru1-N3	159.4(4)	159.17(13)	158.01	158.10
N4-Ru1-N5	79.4(4)	79.7(4)	86.45	86.47
λ [c]	3.65	2.73	2.46	3.63
σ^2 [d]	60.3	59.8	46.4	46.1

[a] data from Chapter 3; [b] data from DFT calculations; [c] $\lambda = \frac{1}{6}\sum_{n=1,6}\left[\frac{d_n - <d>}{<d>}\right]^2$, mean quadratic elongation where d_n is one of the six bond lengths calculated by DFT and <d> is the mean of those bond lengths; [d] $\sigma^2 = \frac{1}{11}\sum_{n=1,12}(\theta_n - 90)^2$, bond angle variance where θ_n is one of the twelve angles calculated by DFT.

4.2.2 Photochemistry

Because of the low water solubility of [**2**]$(PF_6)_2$ the PF_6^- counter ions were exchanged to Cl^- (see experimental section for details), to be able to study the photochemistry in aqueous solution. In aqueous solution, the two complexes [**2**]Cl_2 and [**4**]$(PF_6)_2$ show a ^{1}MLCT absorption band at 470 and 485 nm, thus, the alkyne functionalization causes a shift of the ^{1}MLCT absorption band to the red region, compared to the non-functionalized analogues [**1**]$(PF_6)_2$ and [**3**]$(PF_6)_2$ (Table 4.2 and Figure AIV.3). DFT studies pointed out that the lowest unoccupied molecular orbitals (LUMOs) of these complexes is the π^* orbital of the tpy ligand, as it is for [Ru(tpy)(bpy)(Hmte)]$(PF_6)_2$ ([**5**]$(PF_6)_2$).[16] The red shift of the MLCT state is caused by the stabilization of this orbital by the electron-withdrawing alkyne substituent (σ_P = 0.23),[17] resulting in a lower energy of the LUMO and therefore, a smaller HOMO – LUMO gap (HOMO = highest occupied molecular orbital). The complexes show very little singlet oxygen generation ($\Phi_\Delta < 0.03$), and their phosphorescence quantum yields are very low ($\Phi_P < 5 \cdot 10^{-4}$, see Table 4.2 and Figure AIV.4).

The photoreactivity of [**2**]Cl_2 and [**4**]$(PF_6)_2$ was investigated by irradiation of solutions of the complexes in water with a green LED (517 nm) at 37 °C and recorded by UV-vis spectroscopy (Figure AIV.5). For each complex, a bathochromic shift of the absorption maxima was observed, typical for the release of the thioether ligand and the formation of the corresponding aqua complex (mass spectrometry data in Figure AIV.6).[18-20] The photosubstitution quantum yields (Φ_{517}) were determined using the Glotaran software package.[21] Φ_{517} Values of 0.022 and 0.080 were obtained for [**2**]Cl_2 and [**4**]$(PF_6)_2$, respectively (Table 4.2 and Figure AIII.7), which are comparable with the values reported for complexes [**1**]$(PF_6)_2$ and [**3**]$(PF_6)_2$ (Chapter 3). Overall, functionalization of tpy with a single alkyne group directly attached at the 4'-position had no significant effect on the photosubstitution properties of the ruthenium complex. Due to potential competition between photosubstitution, phosphorescence, and singlet oxygen production in ruthenium polypyridyl complexes, the observation of excellent photosubstitution quantum yields mean that these PACT complexes are essentially non-emissive, and thus cannot be visualized in cells by optical microscopy.

Table 4.2. Lowest-energy absorption maxima (λ_{max} in nm) in MilliQ water, molar absorption coefficients at λ_{max} (ε_{max} in $M^{-1} \cdot cm^{-1}$) in MilliQ water, phosphorescence quantum yields (Φ_P) in methanol-d_4, singlet oxygen quantum yields (Φ_Δ) in methanol-d_4, and photosubstitution quantum yields (Φ_{517}) in MilliQ water for complexes [**1**]X_2 – [**4**]X_2.

complex	NN	R	λ_{max} (ε_{max}) [a]	Φ_P [b]	Φ_Δ [b]	Φ_{517} [a]
[**1**]$(PF_6)_2$ [c]	i-biq	H	429 ($5.76 \cdot 10^3$)	$1.5 \cdot 10^{-4}$	0.010	0.023
[**2**]Cl_2	i-biq	CCH	470 ($7.65 \cdot 10^3$)	$2.4 \cdot 10^{-4}$	0.017	0.022
[**3**]$(PF_6)_2$ [c]	i-Hdiqa	H	470 ($5.35 \cdot 10^3$)	$4.5 \cdot 10^{-4}$	0.042	0.077
[**4**]$(PF_6)_2$	i-Hdiqa	CCH	485 ($6.86 \cdot 10^3$)	$< 1.0 \cdot 10^{-4}$	0.010	0.080

[a] in MilliQ water; [b] in methanol-d_4; [c] data from Chapter 3.

4.2.3 Cytotoxicity and cellular uptake

All ruthenium complexes were found to be thermally stable in cell growing medium (OptiMEM complete) when kept in the dark at 37 °C for 24 h (Figure AIV.8). The cytotoxicity of complexes [**2**]Cl_2 and [**4**]$(PF_6)_2$ was then tested under normoxic conditions (21% O_2) in human lung carcinoma (A549) and human epidermoid carcinoma (A431) cell lines. Prodrug incubation for 24 h in the dark was followed by light activation (green LED, 520 nm, 38 J/cm^2, for 30 min) (Figure AIV.9), and incubation of the cells with the activated drug for an additional 48 h.[22] A sulforhodamine B (SRB) assay was performed at t = 96 h to compare cell proliferation in treated *vs.* untreated cells. The dose response curves are shown in Figure AIV.10, the effective concentrations to inhibit cell growth (EC_{50} values) as well as the ratio of the EC_{50} values obtained in the dark and that under light irradiation, also called the photo index (PI), are reported in Table 4.3.

In the dark, the cytotoxicity of [**2**]Cl_2 was comparable to its non-functionalized analogue [**1**]$(PF_6)_2$ (66 *vs.* 79 μM), while [**4**]$(PF_6)_2$ was twice as toxic as [**3**]$(PF_6)_2$ (29 *vs.* 62 μM). After light activation, both complexes showed increased cytotoxicity with similar EC_{50} values (5 and 7 μM for [**2**]Cl_2 and [**4**]$(PF_6)_2$, respectively). These values are lower than that of their corresponding non-functionalized analogues. Interestingly, while the PI for both i-Hdiqa-based complexes is 4, alkyne functionalization of the i-biq complex led to an increase of the PI from 4 to 12. Thus, the effect of the alkyne group on the EC_{50} values is different for the two complexes. Overall, alkyne functionalization in [**2**]Cl_2 and [**4**]$(PF_6)_2$ led to an increased cytotoxicity compared to their non-functionalized analogues [**1**]$(PF_6)_2$ and [**3**]$(PF_6)_2$ in the dark and after light activation.

Table 4.3. (Photo)cytotoxicity (EC_{50} with 95% confidence interval in μM)[a] and cellular uptake (CU with mean deviation in nmol Ru/mg cell protein)[b] of [**1**]X_2 – [**4**]X_2 in lung cancer cells (A549) under normoxic conditions (21% O_2).

	[1](PF$_6$)$_2$		**[2]Cl$_2$**		**[3](PF$_6$)$_2$**		**[4](PF$_6$)$_2$**	
R	H		CCH		H		CCH	
dark	79.7	+6.1 −5.7	66.0	+12.4 −9.9	62.1	+16.4 −13.8	29.4	+2.7 −2.4
light	20.6	+3.0 −2.6	5.3	+1.4 −1.1	13.8	+4.3 −3.6	7.0	+1.5 −1.3
PI[c]	3.9		12.5		4.5		4.2	
CU	0.32 ± 0.14		0.73 ± 0.12		0.69 ± 0.16		1.19 ± 0.20	

[a] The (photo)cytotoxicity experiments were performed in biological and technical triplicates; [b] Cell uptake upon incubation for 24 h with 30 μM drug. Results are averaged over three independent experiments; [c] the photo index (PI) is defined as $EC_{50,\,dark}/EC_{50,\,light}$.

Cell uptake experiments in A549 cancer cells were undertaken to explain the different cytotoxicity behavior of the complexes. The concentration of ruthenium in nmol per mg cell protein was determined by high-resolution continuum-source atomic absorption spectrometry (HRCS AAS) after incubation of the cells for 24 h with 30 μM drug in the dark. The results revealed that the alkyne-functionalized complexes [**2**]Cl_2 and [**4**](PF$_6$)$_2$ were taken up twice as much in A549 cells than their non-functionalized analogues [**1**](PF$_6$)$_2$ and [**3**](PF$_6$)$_2$ (Table 4.4). For [**4**](PF$_6$)$_2$, the doubled concentration in the cells correlates well to a halved EC_{50} value, found both in the dark and after light activation (PI stays at 4). Therefore, the cytotoxicity can directly be correlated to the cellular uptake and the amount of ruthenium present in the cells. For [**2**]Cl_2, doubling the amount of ruthenium taken up in the cells had only little effect on its dark cytotoxicity. After light activation, however, the EC_{50} value of [**2**]Cl_2 was reduced to a quarter of the corresponding EC_{50} value of [**1**](PF$_6$)$_2$. Therefore, it can be concluded that i) the alkyne functionalization has a significant effect on the cell uptake of both complexes and thus on their cytotoxicity, and that ii) [**2**]Cl_2 is a better prodrug than [**4**](PF$_6$)$_2$. In the dark, it showed only little cytotoxic interactions with biological targets compared to [**4**](PF$_6$)$_2$. In addition, while [**2**]Cl_2 is taken up in cells in lower amounts than [**4**](PF$_6$)$_2$, both complexes show similar EC_{50} values after light activation. The differences in dark and light cytotoxicity of complexes [**2**]Cl_2 and [**4**](PF$_6$)$_2$ point out that depending on the bidentate ligand, the complexes interact differently in the cells and thus, probably possess different biological targets or mode of actions.

4.2.4 Subcellular localization of the ruthenium complexes

To shed light on the different cytotoxic behaviors of these PACT agents, more insight into their cellular distribution and resulting target interactions is required. Since the PACT agents are non-emissive, these complexes need to be labeled with a fluorophore moiety to be visualized in cells. The alkyne handle of [**2**]Cl_2 and [**4**]$(PF_6)_2$ offers the opportunity to label the compounds *via* click chemistry after cell treatment. Azide-alkyne copper-catalyzed cycloaddition (CuAAC) with azide AlexaFluor™ 488 in fixed and permeabilized A549 lung cancer cells 24 h after green light activation were performed on [**2**]Cl_2 and [**4**]$(PF_6)_2$, according to a protocol established by DeRose and coworkers (Figure AIV.11).[12] Confocal microscopy was applied for the imaging of the complexes.

At concentrations equal to their EC_{50} values (5 and 7 μM), no fluorescence signal was observed for [**2**]Cl_2 and [**4**]$(PF_6)_2$, respectively (data not shown). Therefore, the prodrug concentrations were increased to 25 μM. As this concentration is highly toxic to the cells, the incubation time after light activation was reduced from 48 to 24 h. By doing so, the cells were stressed but survived and could be imaged. The fluorescence signal was located outside the nucleus, in the cytoplasm (Figure 4.2), and appeared as little dots, mainly on one side of the nucleus. This observation can be taken as an indication for a different mode of action of [**2**]Cl_2 and [**4**]$(PF_6)_2$ compared to DNA-interacting ruthenium complexes (Figure AIV.12 and AIV.13).[23, 24] The localization of the signals for [**2**]Cl_2 and [**4**]$(PF_6)_2$ were found to be identical (results for [**2**]Cl_2 shown in Figure AIV.14), but the fluorescence signal intensity of [**2**]Cl_2 was weaker, which correlates to the lower uptake of [**2**]Cl_2 compared to [**4**]$(PF_6)_2$ (see Table 4.3). In the absence of catalytic copper (Cu-, Figure 4.2) and any ruthenium complex, no fluorescent signal was observed, indicating that the click reaction is selective for the complex and background fluorescence was minimal. Without light, the complexes are not activated and should not covalently interact with their targets. This was confirmed by the lower signal, due to washing out of the fluorophore-labeled complexes of the permeabilized cells, a procedure needed for labelling before microscopy. Overall, the alkyne handle on the complexes allowed for labeling of [**2**]Cl_2 and [**4**]$(PF_6)_2$ with Alexa Fluor™ 488 inside fixed cells.

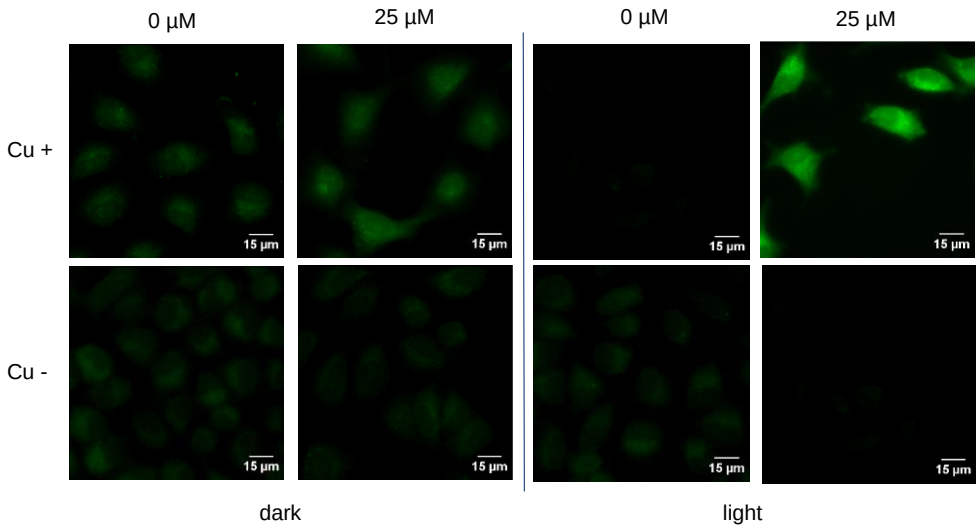

Figure 4.2. Confocal images of fluorescent labeling of A549 cancer cell lines treated for 24 h with 0 or 25 µM of [**4**](PF$_6$)$_2$ after fixation, permeabilization, and CuAAC-based labeling with Alexa Fluor™ 488 azide, either with or without light activation. Cu-free controls show no fluorescence. Bar represents 15 µm.

This encouraging result was used to further investigate the intracellular localization of [**4**](PF$_6$)$_2$. Co-staining of cell compartments in the cytoplasm were hence undertaken after treatment with the ruthenium compound. Possible targets within the cytoplasm are hydrophobic organelles such as mitochondria, endoplasmic reticulum (ER), lysosomes, and Golgi apparatus. Mitochondria are well-known targets for lipophilic, charged ruthenium polypyridyl complexes. Recently, the weakly emissive tpy-based ruthenium complex [Ru(tpy)(dppn)(X)](PF$_6$)$_2$ (where dppn = benzo[i]dipyrido-[3,2-a:2′,3′-c]phenazine and X = a thioether-glucose conjugate) was localized in this subcellular organelle.[25] Comparison of the localization and structure of the fluorescent signal of this complex with the results obtained for [**4**](PF$_6$)$_2$ showed that the distribution of our compound is different. Thus, mitochondria were excluded as possible target for [**4**](PF$_6$)$_2$. In addition, examples of ruthenium complexes that cause ER stress have been reviewed recently.[26] Here as well, the ER was excluded as target for [**4**](PF$_6$)$_2$, based on the structure of the observed compartment (Figure AIV.15). Lysosomes, however, seemed to be likely subcellular targets from the observed emission patterns, and therefore, co-staining of these cell compartments was undertaken using immunostaining of lysosomal-associated membrane protein 1 (LAMP1). As shown in Figure 4.3, the fluorescent signal corresponding to the lysosome stain (in red) was

localized close to the nucleus in the cytoplasm, but the fluorescence of the complex (in green) did not significantly overlap with these signals, indicating that [**4**]$(PF_6)_2$ did not co-localize in the lysosomes. Co-localization quantification for the immunostaining (Pearson coefficient) was attempted but the resolution of the images was too low to obtain reliable results. Thus, after ruling out all these organelles, and considering the shape of the emission signal, it is hypothesized that [**4**]$(PF_6)_2$ localizes in the Golgi apparatus. To confirm this hypothesis, co-staining of this cell compartment must be undertaken.

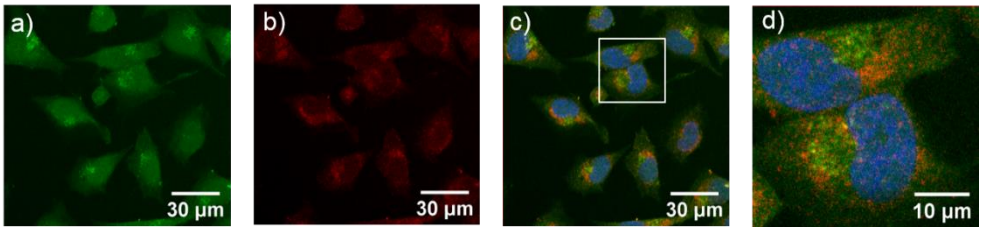

Figure 4.3. Confocal images of fluorescent labeling of A549 cancer cell lines treated with 25 µM of [**4**]$(PF_6)_2$ after fixation and permeabilization. a) labeling of [**4**]$(PF_6)_2$ with Alexa Fluor™ 488 azide (green), b) antibody staining of LAMP1 for lysosomes with 647 dye (red), c) overlay of LAMP1, [**4**]$(PF_6)_2$, and nucleus staining (with Hoechst in blue), and d) zoom of c).

The Golgi apparatus is a membrane-coated cell organelle close to the endoplasmic reticulum near the nucleus. It plays an important role in the intracellular traffic of lysosomal and secretory materials, and it is responsible for the processing and packaging of proteins.[27] The Golgi apparatus has repeatedly been suggested as target of luminescent ruthenium compounds when the fluorescence is located in perinuclear regions,[28] but strong evidence of subcellular organelle localization is often missing.[29] Luminescent probes based on rhenium and iridium, however, proved to accumulate in the Golgi apparatus.[30, 31] To the best of our knowledge, the Golgi apparatus was not yet pointed out as target for ruthenium-based anticancer compounds. Nevertheless, the subcellular organelle does play a central role in the trafficking and processing of the anticancer compound cisplatin. Molenaar *et al.* reported on a fluorophore-functionalized cisplatin derivative still present in the Golgi apparatus of human bone osteosarcoma epithelial cells (U2-OS) after 24 h, while not localized in the nucleus anymore.[4] In human ovarian carcinoma cells, fluorescein-labeled cisplatin was also found to pass through the Golgi apparatus.[6] The metal complex was transported *via* lysosomal vesicles to the Golgi and then further from Golgi associated vesicles into the secretory pathway, leading to the efflux of the complex. On the other hand, Liang *et al.* demonstrated that in human

epidermoid carcinoma cells (KB-3-1) Alexa-labeled cisplatin accumulates first in the Golgi apparatus, before it is transferred to the nucleus.[32] In addition, transport from the Golgi compartment to the nucleus is decelerated in KB cisplatin-resistant cells, which suggests a failure of proper trafficking within these cells. To conclude, the Golgi apparatus strongly participates in vesicle transportation, and thus can be an effective target for anticancer compounds. As above mentioned examples with cisplatin pointed out, an involvement in metal transportation is highly possible, in the early stages of drug uptake as well as drug efflux. Therefore, time dependent fluorescent imaging experiment will need to be undertaken for [**2**]Cl_2 and [**4**]$(PF_6)_2$ to follow the drug *in cellulo* to understand their intracellular trafficking and processing.

4.3 Conclusions

Two new alkyne-functionalized ruthenium-based PACT agents were synthesized. This small modification, made of only two atoms directly connected to the prodrug, had no significant effect on the X-ray structure and photosubstitution properties of the complexes. However, it results in doubling of the cellular uptake of both complexes, which influenced their cytotoxicity. Still, such alkyne group appears as a promising method to monitor the fate of non-emissive PACT compounds in cells, while minimally influencing their biological properties. The alkyne handles indeed allowed for the labeling of the complexes with a fluorophore moiety in fixed cells, *i.e.*, after the drug has distributed inside the cell and interacted with its cellular target. With this method, it was possible to i) visualize the light-dependent activation of the complexes inside cells, as the non-activated prodrug was washed away during the procedure to not appear on the microscopy images, ii) localize the complexes intracellularly, and in particular demonstrating that it stays outside the nucleus, and probably resides, after 24 h, in the Golgi apparatus. The latter suggests that the mode of action of these ruthenium-based PACT agents is DNA independent and thus, different from that of cisplatin. To obtain more information about the mode of action of the complexes, it will be necessary to investigate the time-dependent cellular distribution and to identify the cellular targets of the complexes. We foresee that the alkyne handles used here to visualize the compound in cells, will also allow for attaching reporter tags to perform pull-down experiments.[13, 14, 33-35]

4.4 Experimental

4.4.1 Methods and Materials

4′-Bromo-2,2′:6′,2″-terpyridine was purchased from TCI Europe; $RuCl_3$ and potassium fluoride from Alfa Aesar; 3-bromoisoquinoline from ABCR; isoquinolin-3-amine, tris(dibenzylideneacetone)dipalladium(0), 1,3-bis(diphenylphosphino)propane, 2-(methylthio)ethanol, and *tert*-butyldimethylsilylethyne from Sigma Aldrich; and potassium *tert*-butoxide from Acros Organics. The ligand i-biq was synthesized according to literature;[36] i-Hdiqa, [**1**]$(PF_6)_2$, and [**3**]$(PF_6)_2$ as described in Chapter 3; and [Ru(HCC-tpy)(bpy)(Hmte)]$(PF_6)_2$ as described in Chapter 2. All metal complexes were synthesized in dim light and stored in darkness. All reactants and solvents were used without further purification. ^{1}H NMR spectra were recorded using a Bruker AV-300 spectrometer. Chemical shifts are indicated in ppm. Mass spectra were recorded using an MSQ Plus Spectrometer.

4.4.2 Synthesis

[Ru(RCC-tpy)(i-biq)(Cl)]Cl (R = TBDMS)

[Ru(RCC-tpy)$(Cl)_3$] (251 mg, 0.445 mmol), i-biq (114 mg, 0.445 mmol), and lithium chloride (105 mg, 2.50 mmol) were dissolved in degassed ethanol/water mixture (3:1, 40 mL). Triethylamine (160 µL, 1.15 mmol) was added and the reaction mixture was refluxed (60 °C) under dinitrogen atmosphere overnight. The reaction mixture was filtered hot over Celite and the cake was washed with ethanol. After evaporation of the solvents, the crude was purified by column chromatography on silica with dichloromethane/methanol (9:1) as eluent (R_f = 0.70). Yield: 73% (260 mg, 0.325 mmol).

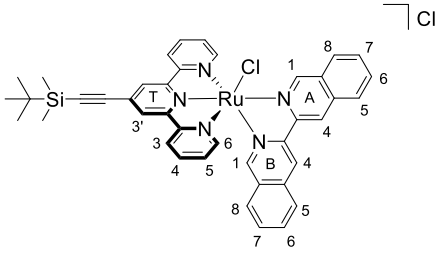

^{1}H NMR (300 MHz, methanol-d_4, 298 K) δ 10.78 (s, 1H, A1), 9.34 (s, 1H, A4), 9.03 (s, 1H, B4), 8.74 (s, 2H, T3′), 8.63 (dd, *J* = 8.0, 1.2 Hz, 2H, T3), 8.46 – 8.32 (m, 2H, A5 + A8), 8.11 – 7.94 (m, 4H, B5 + B1 + A6 + A7), 7.94 – 7.82 (m, 4H, T4 + T6), 7.78 – 7.65 (m, 2H, B6 + B8), 7.57 (ddd, *J* = 8.2, 6.8, 1.1 Hz, 1H, B7), 7.29 (ddd, *J* = 7.6, 5.6, 1.3 Hz, 2H, T5), 1.15 (s, 9H, Si-C-($C\underline{H}_3$)$_3$), 0.34 (s, 6H, Si-($C\underline{H}_3$)$_2$). *^{13}C NMR (75 MHz, methanol-d_4, 298 K)* δ 158.7 + 158.6 (C_q T2 + T2′), 155.5 (A1), 154.7 (A6), 151.6 (T6), 149.5 (C_q A3 or B3), 137.0 (T4), 135.5 + 134.4 (C_q A4a + B4a), 132.4 (B5), 132.1 (B6), 129.9 (A7), 129.4 (B7), 128.9 (C_q A8a or B8a), 127.6 (A5), 127.4 (A8), 127.3 (T5), 127.0 (B1), 126.0 (B8), 124.2 (T3′), 123.9 (T3), 120.1 (A4), 119.5 (B4), 102.6 + 100.2 (C_q C$\underline{C}$H + $\underline{C}$CH), 25.2 (Si-C-($\underline{C}H_3$)$_3$), -6.0 (Si-($\underline{C}H_3$)$_2$), four quaternary carbons are missing: C_q A3 or B3, C_q A8a or B8a, C_q Si-$\underline{C}$-(CH_3)$_3$, C_q T4′. *ES MS m/z (calc.):* 764.6 (764.2, $[M - Cl]^+$).

[Ru(RCC-tpy)(i-Hdiqa)(Cl)]Cl (R = TBDMS)

[Ru(RCC-tpy)$(Cl)_3$] (400 mg, 0.709 mmol), i-Hdiqa (192 mg, 0.709 mmol), and lithium chloride (165 mg, 3.94 mmol), were dissolved in degassed ethanol/water mixture (3:1, 64 mL). Triethylamine (252 µL, 1.81 mmol) was added and the reaction mixture was refluxed (60 °C) under dinitrogen atmosphere for 5 h. The reaction mixture was filtered hot over Celite and the cake was washed with ethanol. After evaporation of the solvents, the crude was purified by column chromatography on silica with dichloromethane/methanol (9:1) as eluent (R_f = 0.74). Yield: 71% (413 mg, 0.507 mmol).

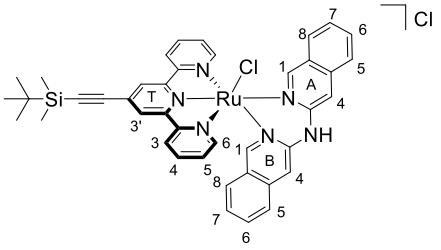

^{1}H NMR (300 MHz, methanol-d_4, 298 K) δ 10.34 (s, 1H, A1), 8.64 (s, 2H, T3'), 8.60 (dd, *J* = 8.0, 1.2 Hz, 2H, T3), 8.58 (ddd, *J* = 5.6, 1.6, 0.7 Hz, 2H, T6), 8.13 (d, *J* = 8.6 Hz, 1H, A8), 8.04 (dd, *J* = 8.5, 1.0 Hz, 1H, A5), 7.99 (td, *J* = 7.8, 1.6 Hz, 2H, T4), 7.88 (s, 1H, A4), 7.85 (ddd, *J* = 8.3, 6.9, 1.2 Hz, 1H, A6), 7.66 – 7.59 (m, 1H, A7), 7.58 – 7.47 (m, 4H, B5 + T5 + B6), 7.45 (s, 1H, B1), 7.39 (d, *J* = 8.3 Hz, 1H, B8), 7.27 (s, 1H, B4), 7.26 – 7.18 (m, 1H, B7), 1.11 (s, 9H, Si-C-(C<u>H</u>$_3$)$_3$), 0.30 (s, 6H, Si-(C<u>H</u>$_3$)$_2$). *^{13}C NMR (75 MHz, methanol-d_4, 298 K)* δ 160.9 + 160.4 (C_q T2 +T2'), 160.0 (A1) 154.5 (T6), 154.3 (B1), 152.3 + 151.3 (C_q A3+ B3), 139.7 + 138.5 (C_q A4a + B4a), 138.5 (T4), 133.7 (A6), 133.5 (B6), 129.1 (C_q T4'), 128.9 (A8), 128.5 (T5), 127.9 + 126.9 (C_q A8a + B8a), 127.7 (A7), 127.5 (B7), 127.4 (B8), 126.8 (A5), 126.1 (B5), 125.6 (T3'), 125.3 (T3), 108.2 (A4), 107.6 (B4), 103.8 + 101.7 (C_q C<u>C</u>H + <u>C</u>CH), 26.6 (Si-C-(<u>C</u>H$_3$)$_3$), 17.6 (C_q Si-<u>C</u>-(CH$_3$)$_3$), -4.6 (Si-(<u>C</u>H$_3$)$_2$). *ES MS m/z (calc.):* 779.5 (779.2, [M – Cl]$^+$).

[Ru(RCC-tpy)(i-biq)(Hmte)](PF$_6$)$_2$ (R = TBDMS)

[Ru(RCC-tpy)(i-biq)(Cl)]Cl (151 mg, 0.189 mmol) and 2-(methylthio)ethanol (1 mL, 11 mmol) were dissolved in a degassed water/acetone mixture (4:1, 25 mL). The resultant mixture was stirred and heated to 60 °C under dinitrogen atmosphere overnight. The reaction mixture was filtered hot over Celite and the cake was washed with ethanol. The amount of solvents was reduced by rotary evaporation. The product was precipitated by addition of saturated hexafluoridophosphate, filtered, and washed with cold water. Yield: 93% (195 mg, 0.176 mmol).

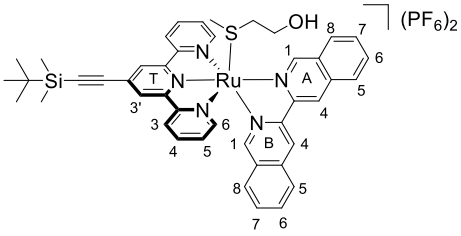

^{1}H NMR (300 MHz, acetone-d_6, 298 K) δ 10.64 (s, 1H, A1), 9.52 (s, 1H, A4), 9.28 (s, 1H, B4), 9.01 (s, 2H, T3'), 8.88 (dt, *J* = 8.0, 1.1 Hz, 2H, T3), 8.49 (dd, *J* = 8.2, 1.2 Hz, 1H, A8), 8.43 (d, *J* = 8.2 Hz, 1H, A5), 8.38 (s, 1H, B1), 8.26 (dd, *J* = 8.0, 1.1 Hz, 2H, T6), 8.20 – 8.09 (m, 4H, T4 + A6 + B5), 8.05 (ddd, *J* = 8.1, 6.9, 1.2 Hz, 1H, A7), 7.84 (ddd, *J* = 8.2, 6.8, 1.3 Hz, 1H, B6), 7.74 (d, *J* = 8.1 Hz, 1H, B8), 7.64 (ddd, *J* = 8.2, 6.8, 1.1 Hz, 1H, B7), 7.50 (ddd, *J* = 7.7, 5.5, 1.3 Hz, 2H, T5), 4.22 (t, *J* = 5.1 Hz, 1H, O<u>H</u>), 3.64 (dt, *J* = 5.6, 5.1 Hz, 2H, S-CH$_2$-C<u>H</u>$_2$), 2.11 (t, *J* = 5.6 Hz, 2H, S-C<u>H</u>$_2$), 1.58 (s, 3H, S-C<u>H</u>$_3$), 1.13 (s, 9H, Si-C-(C<u>H</u>$_3$)$_3$), 0.36 (s, 6H, Si-(C<u>H</u>$_3$)$_2$). *^{13}C NMR (75 MHz, acetone-d_6, 298 K)* δ 159.0 + 158.7 (C_q T2 + T2'), 156.6 (A1), 154.8 (B1), 154.3 (T6), 150.7 + 150.2 (C_q A3 + B3), 139.8 (T4), 136.8 + 136.2 (C_q A4a + B4a), 134.2 (A6), 134.1 (B6), 131.4 + 130.7 (C_q A8a + B8a), 131.2 (A7), 130.7 (B7), 129.8 (C_q T4'), 129.7 (T5), 129.0 (A8), 128.7 (B8), 128.4 (A5), 128.3 (B5), 127.1 (T3'), 126.3 (T3), 122.2 (A4), 121.5 (B4), 103.2 + 103.0 (C_q C<u>C</u>H + <u>C</u>CH), 59.0 (S-CH$_2$-<u>C</u>H$_2$), 38.1 (S-<u>C</u>H$_2$), 26.5 (Si-C-(<u>C</u>H$_3$)$_3$), 17.3 (C_q Si-<u>C</u>-(CH$_3$)$_3$), 14.7 (S-<u>C</u>H$_3$), -4.6 (Si-(<u>C</u>H$_3$)$_2$). *ES MS m/z (calc.):* 410.5 (410.6, [M – 2PF$_6$]$^{2+}$).

[Ru(RCC-tpy)(i-Hdiqa)(Hmte)](PF$_6$)$_2$ (R = TBDMS)

[Ru(RCC-tpy)(i-Hdiqa)(Cl)]Cl (300 mg, 0.368 mmol) and 2-(methylthio)ethanol (2 mL, 22 mmol) were dissolved in a degassed water/acetone mixture (4:1, 50 mL). The resultant mixture was stirred and heated to 60 °C under dinitrogen atmosphere overnight. The reaction mixture was filtered hot over Celite and the cake was washed with ethanol. The amount of solvents was reduced by rotary evaporation. The

product was precipitated by addition of saturated hexafluoridophosphate, filtered, and washed with cold water. Yield: 95% (395 mg, 0.351 mmol).

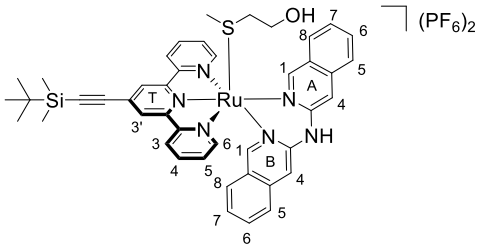

^{1}H NMR (300 MHz, acetone-d_6, 298 K) δ 10.16 (s, 1H, A1), 9.64 (s, 1H, NH), 8.95 (dd, *J* = 5.6, 1.6 Hz, 2H, T6), 8.91 (s, 2H, T3'), 8.87 (dd, *J* = 8.1, 1.4 Hz, 2H, T3), 8.35 (dd, *J* = 8.4, 1.1 Hz, 1H, A8), 8.28 (td, *J* = 7.9, 1.5 Hz, 2H, T4), 8.15 (dd, *J* = 8.5, 1.0 Hz, 1H, A5), 8.10 (s, 1H, A4), 7.95 (ddd, *J* = 8.3, 6.8, 1.2 Hz, 1H, A6), 7.82 (s, 1H, B1), 7.81 – 7.70 (m, 4H, T5 + B5 + A7), 7.63 (ddd, *J* = 8.4, 6.7, 1.2 Hz, 1H, B6), 7.58 (s, 1H, B4), 7.54 (dd, *J* = 8.4, 1.1 Hz, 1H, B8), 7.32 (ddd, *J* = 8.3, 6.7, 1.2 Hz, 1H, B7), 4.06 (t, *J* = 5.1 Hz, 1H, OH), 3.50 (dt, *J* = 5.6, 5.1 Hz, 2H, S-CH$_2$-CH$_2$), 1.92 (t, *J* = 5.6 Hz, 2H, S-CH$_2$), 1.39 (s, 3H, S-CH$_3$), 1.09 (s, 9H, Si-C-(CH$_3$)$_3$), 0.31 (s, 6H, Si-(CH$_3$)$_2$). *^{13}C NMR (75 MHz, acetone-d_6, 298 K)* δ 159.5 + 159.0 (C_q T2 + T2'), 159.1 (A1), 155.7 (T6), 153.0 (B1), 151.4 + 150.9 (C_q A3 + B3), 139.9 (T4), 139.5 + 138.6 (C_q A4a + B4a), 134.1 (A6), 134.0 (B6), 131.0 (C_q T4'), 129.4 (T5), 129.0 (A8), 128.3 (B8), 128.3 + 126.8 (C_q A8a + B8a) 127.9 (A7), 127.4 (B7), 127.1 (T3'), 126.7 (A4), 126.4 (T3), 126.1 (B5), 110.3 (A4), 109.0 (B4), 103.0 (C_q CCH or CCH), 58.9 (S-CH$_2$-CH$_2$), 37.8 (S-CH$_2$), 26.5 (Si-C-(CH$_3$)$_3$), 17.3 (C_q Si-C-(CH$_3$)$_3$), 15.0 (S-CH$_3$), -4.7 (Si-(CH$_3$)$_2$), one quaternary carbon is missing: C_q CCH or CCH. *ES MS m/z (calc.):* 417.8 (418.1, $[M - 2PF_6]^{2+}$).

[Ru(HCC-tpy)(i-biq)(Hmte)](PF$_6$)$_2$, [2](PF$_6$)$_2$

A solution of [Ru(RCC-tpy)(i-biq)(Hmte)](PF$_6$)$_2$ (120 mg, 0.108 mmol) in methanol (5 mL) was combined with a solution of potassium fluoride (63 mg, 1.1 mmol) in methanol (5 mL). The resulting reaction mixture was stirred at 30 °C overnight. The amount of solvent was reduced by rotary evaporation and aqueous potassium hexafluoridophosphate was added dropwise to the solution till a precipitate was formed. The precipitate was filtered and washed with cold water. Yield: 82% (88 mg, 0.089 mmol).

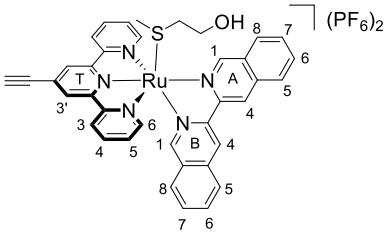

^{1}H NMR (300 MHz, acetone-d_6, 298 K) δ 10.65 (s, 1H, A1), 9.53 (s, 1H, A4), 9.29 (s, 1H, B4), 9.03 (s, 2H, T3'), 8.88 (d, *J* = 8.1 Hz, 2H, T3), 8.50 (d, *J* = 8.1 Hz, 1H, A8), 8.43 (d, *J* = 8.2 Hz, 1H, A5), 8.34 (s, 1H, B1), 8.27 (d, *J* = 5. Hz, 2H, T6), 8.23 – 8.01 (m, 5H, T4 + A6 + B5 + A7), 7.85 (ddd, *J* = 8.2, 6.7, 1.4 Hz, 1H, B6), 7.72 (d, *J* = 8.2 Hz, 1H, B8), 7.64 (ddd, *J* = 8.2, 6.8, 1.1 Hz, 1H, B7), 7.51 (ddd, *J* = 7.7, 5.5, 1.3 Hz, 2H, T5), 4.59 (s, 1H, CCH), 4.26 (t, *J* = 4.7 Hz, 1H, OH), 3.63 (dt, *J* = 5.6, 4.7 Hz, 2H, S-CH$_2$-CH$_2$), 2.12 (t, *J* = 5.6 Hz, 2H, S-CH$_2$), 1.59 (s, 3H, S-CH$_3$). *^{13}C NMR (75 MHz, acetone-d_6, 298 K)* δ 159.0 + 158.7 (C_q T2 + T2'), 156.6 (A1), 154.8 (B1), 154.4 (T6), 150.8 + 150.2 (C_q A3 + B3), 139.8 (T4), 136.8 + 136.2 (C_q A4a + B4a), 134.2 (A6), 134.2 (B6), 131.2 (A7), 131.0 + 130.7 + 129.8 (C_q A8a + B8a + T4'), 130.7 (B7), 129.7 (T5), 129.1 (A8), 128.7 (A5), 128.4 + 128.3 (B5 + B8), 127.4 (T3'), 126.3 (T3), 122.2 (A4), 121.4 (B4), 87.9 (CCH), 81.3 (C_q CCH), 58.9 (S-CH$_2$-CH$_2$), 38.1 (S-CH$_2$), 14.8 (S-CH$_3$). *ES MS m/z (calc.):* 354.0 (353.6, $[M - 2PF_6]^{2+}$).

[Ru(HCC-tpy)(i-biq)(Hmte)]Cl$_2$, [2]Cl$_2$

[**2**](PF$_6$)$_2$ (65 mg, 0.065 mmol) was dissolved in a minimum amount of acetone (1 mL) and saturated Bu$_4$NCl solution (4 mL) was added dropwise. The formed precipitate was filtered and washed several times with acetone. The product was obtained as brownish red solid. Yield: 99% (50 mg, 0.064 mmol).

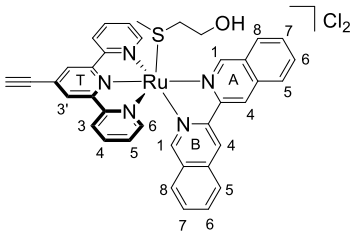

^{1}H NMR (300 MHz, methanol-d_4, 298 K) δ 10.53 (s, 1H, A1), 9.43 (s, 1H, A4), 9.19 (s, 1H, B4), 8.97 (s, 2H, T3'), 8.71 (dt, *J* = 7.9, 1.1 Hz, 2H, T3), 8.49 (d, *J* = 8.1 Hz, 1H, A8), 8.42 (d, *J* = 7.9 Hz, 1H, A5), 8.16 – 7.98 (m, 6H, A6 + B5 + T4 + B1 + A7), 7.94 (dd, *J* = 5.5, 1.5 Hz, 2H, T6), 7.89 – 7.78 (m, 2H, B8 + B6), 7.65 (ddd, *J* = 7.8, 6.5, 1.1 Hz, 1H, B7), 7.42 (ddd, *J* = 7.7, 5.5, 1.3 Hz, 2H, T5), 4.53 (s, 1H, CC<u>H</u>), 3.61 – 3.46 (m, 2H, S-CH$_2$-C<u>H$_2$</u>), 1.98 – 1.80 (m, 2H, S-C<u>H$_2$</u>), 1.42 (s, 3H, S-C<u>H$_3$</u>). *^{13}C NMR (214 MHz, methanol-d_4, 298 K)* δ 159.3 + 159.1 (C$_q$ T2 + T2'), 156.8 (A1), 154.5 (B1), 154.2 (T6), 151.0 + 150.5 (C$_q$ A3 + B3), 140.2 (T4), 137.3 + 136.7 (C$_q$ A4a + B4a), 134.6 + 134.5 (A6 + B6), 132.1 (C$_q$ A8a), 131.6 (A7), 131.2 (B7), 130.3 (C$_q$ A8b), 130.0 (T5), 129.2 (A8), 129.0 (A5), 128.6 + 128.6 (B8 + B5), 127.8 (T3'), 126.6 (T3), 122.6 (A4), 121.9 (B4), 88.0 (C<u>C</u>H), 81.0 (C$_q$ <u>C</u>CH), 58.6 (S-CH$_2$-<u>C</u>H$_2$), 38.4 (S-<u>C</u>H$_2$), 14.3 (S-<u>C</u>H$_3$). *High resolution ES MS m/z (calc.):* 353.56450 (353.56457, [M – 2 Cl]$^{2+}$). *Elem. Anal. Calc. for C$_{38}$H$_{31}$Cl$_2$N$_5$ORuS + 3 H$_2$O:* C, 54.87; H, 4.48; N, 8.42. *Found:* C, 54.08; H, 4.08; N, 8.39.

[Ru(HCC-tpy)(i-Hdiqa)(Hmte)](PF$_6$)$_2$, [4](PF$_6$)$_2$

A solution of [Ru(RCC-tpy)(i-Hdiqa)(Hmte)](PF$_6$)$_2$ (200 mg, 0.178 mmol) in methanol (10 mL) was combined with a solution of potassium fluoride (103 mg, 1.78 mmol) in methanol (5 mL). The resulting reaction mixture was stirred at 30 °C overnight. The amount of solvent was reduced by rotary evaporation and aqueous potassium hexafluoridophosphate was added dropwise to the solution till a precipitate was formed. The precipitate was filtered and washed with cold water. The product was obtained as brownish red solid. Yield: 83% (150 mg, 0.148 mmol).

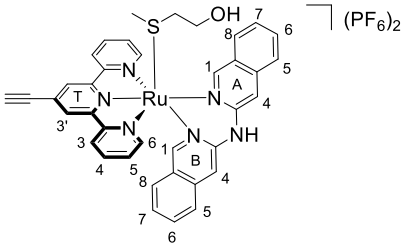

^{1}H NMR (300 MHz, acetone-d_6, 298 K) δ 10.17 (s, 1H, A1), 9.66 (s, 1H, N<u>H</u>), 8.96 (dd, *J* = 5.6, 1.6 Hz, 2H, T6), 8.93 (s, 2H, T3'), 8.87 (dd, *J* = 8.2, 1.4 Hz, 2H, T3), 8.36 (dd, *J* = 8.3, 1.1 Hz, 1H, A8), 8.30 (td, *J* = 7.9, 1.5 Hz, 2H, T4), 8.15 (dd, *J* = 8.6, 1.1 Hz, 1H, A5), 8.11 (s, 1H, A4), 7.95 (ddd, *J* = 8.3, 6.8, 1.2 Hz, 1H, A6), 7.80 (s, 1H, B1), 7.79 – 7.70 (m, 4H, T5 + B5 + A7), 7.63 (ddd, *J* = 8.4, 6.7, 1.2 Hz, 1H, B6), 7.58 (s, 1H, B4), 7.53 (dd, *J* = 8.5, 1.0 Hz, 1H, B8), 7.32 (ddd, *J* = 8.2, 6.7, 1.2 Hz, 1H, B7), 4.52 (s, 1H, CC<u>H</u>), 4.07 (t, *J* = 5.1 Hz, 1H, -O<u>H</u>), 3.50 (dt, *J* = 5.6, 5.1 Hz, 2H, S-CH$_2$-C<u>H$_2$</u>), 1.93 (t, *J* = 5.6 Hz, 2H, S-C<u>H$_2$</u>), 1.39 (s, 3H, S-C<u>H$_3$</u>). *^{13}C NMR (75 MHz, acetone-d_6, 298 K)* δ 159.6 + 159.0 (C$_q$ T2 + T2'), 159.1 (A1), 155.7 (T6), 152.9 (B1), 151.4 + 150.9 (C$_q$ A3 + B3), 140.0 (T4), 139.5 + 138.6 (C$_q$ A4a + B4a), 134.1 (A6), 134.0 (B6), 130.7 (C$_q$ T4'), 129.4 (T5), 129.0 (A8), 128.3 + 126.8 (C$_q$ A8a + B8a), 128.3 (B8), 127.9 (A7), 127.4 (B7), 127.4 (T3'), 126.7 (A5), 126.4 (T3), 126.1 (B5), 110.3 (A4), 108.9 (B4), 87.9 (C<u>C</u>H), 81.1 (C$_q$ <u>C</u>CH), 59.0 (S-CH$_2$-<u>C</u>H$_2$), 37.9 (S-<u>C</u>H$_2$), 15.0 (S-<u>C</u>H$_3$). *ES MS m/z (calc.):* 361.0 (361.1, [M – 2PF$_6$]$^{2+}$). *High resolution ES MS m/z (calc.):* 361.06995 (361.07001, [M – 2PF$_6$]$^{2+}$). *Elem. Anal. Calc. for C$_{38}$H$_{32}$F$_{12}$N$_6$OP$_2$RuS:* C, 45.11; H, 3.19; N, 8.31. *Found:* C, 44.54; H, 3.24; N, 8.20.

4.4.3 Single Crystal X-Ray crystallography

Single crystals of [**2**](PF$_6$)$_2$ were obtained by recrystallization through liquid-vapor diffusion using cyclopentane as solvent and diethyl ether as counter-solvent. In short, 1 mg of [**2**](PF$_6$)$_2$ was dissolved in cyclopentane (1 mL) and placed in a small vial. This vial was placed in a larger vial containing diethyl ether (2.8 mL). The large vial was closed and vapor diffusion within a few days afforded X-ray quality crystals.

All reflection intensities were measured at 110(2) K using a SuperNova diffractometer (equipped with Atlas detector) with Cu *Kα* radiation (*λ* = 1.54178 Å) under the program CrysAlisPro (Version CrysAlisPro 1.171.39.29c, Rigaku OD, 2017). The same program was used to refine the cell dimensions and for data reduction. The structure was solved with the program SHELXS-2014/7 (Sheldrick, 2015) and was refined on F^2 with SHELXL-2014/7 (Sheldrick, 2015). Analytical numeric absorption correction using a multifaceted crystal model was applied using CrysAlisPro. The temperature of the data collection was controlled using the system Cryojet (manufactured by Oxford Instruments). The H atoms were placed at calculated positions using the instructions AFIX 23, AFIX 43, AFIX 137, AFIX 147 or AFIX 163 with isotropic displacement parameters having values 1.2 or 1.5 *U*eq of the attached C or O atoms.

The structure of [**2**](PF$_6$)$_2$ is partly disordered.
The 3,3'-biquinoline ligand and one of the two PF$_6^-$ counter ions are found to be disordered over two orientations, and the occupancy factors of the major components of the disorder refine to 0.54(3) and 0.699(17). [**2**](PF$_6$)$_2$: 0.07 × 0.04 × 0.02 mm^3, triclinic, *P*-1, a = 9.6220 (3), b = 11.2316 (4), c = 19.3633 (7) Å, α = 97.533 (3), β = 92.211 (3), γ = 109.604 (3)°, V = 1946.63 (12) Å^3, Z = 2, μ = 5.43 mm^{-1}, transmission factor range: 0.779–0.924. 25285 Reflections were measured up to a resolution of (sin θ/λ)max = 0.616 Å^{-1}. 7581 Reflections were unique (R_{int} = 0.058), of which 6081 were observed [I > 2σ(I)]. 761 Parameters were refined using 1434 restraints. R1/wR2 [I > 2σ(I)]: 0.0428/ 0.1013. R1/wR2 [all refl.]: 0.0609/ 0.1119. S = 1.02. Residual electron density found between −0.57 and 0.80 e Å^{-3}.

4.4.4 DFT Calculations

DFT was used to perform electronic structure calculations. The structure of [**2**]$^{2+}$ and [**4**]$^{2+}$ was optimized using ADF from SCM,[37] the PBE0 hybrid functional, a triple zeta basis set (TZP) for all atoms, and COSMO to simulate solvent effects in water. The nuclear coordinates (Å) of [**2**]$^{2+}$ and [**4**]$^{2+}$ are given in Table AIV.2 and AIV.3, respectively.

4.4.5 Irradiation experiments monitored with MS and UV-vis

Photoreactions monitored with UV-vis spectroscopy were performed using a Cary Varian spectrometer equipped with temperature control set to 310 K and a magnetic stirrer. The measurements were performed in a quartz cuvette, containing 3 mL of solution. The stirred sample was irradiated perpendicularly to the axis of the spectrometer with the beam of an LED fitted to the top of the cuvette.

For photoactivation with green light, an LED light source (λ = 517 nm, $\Delta\lambda_{1/2}$ = 23 nm, 5.2 mW, $5.43 \cdot 10^{-8}$ mol $\cdot$ s^{-1}) was used, an absorption spectrum was measured every 30 sec until the end of the experiment. [Ru]$_0$ = 0.074, 0.077, 0.061, and 0.127 mM for [**1**](PF$_6$)$_2$, [**2**]Cl$_2$, [**3**](PF$_6$)$_2$, and [**4**](PF$_6$)$_2$, respectively. The data were analyzed using Microsoft Excel. Mass spectrometry was performed at the beginning and at the end of the irradiation to confirm the nature of the reagent and products. Photosubstitution quantum yield calculations were performed using the Glotaran Software package as described in Appendix I. The conditions are summarized in Table AIV.1.

4.4.6 Cytotoxicity and cellular uptake

Cytotoxicity assays and cellular uptake experiments were performed using the protocols described in Appendix I.

4.4.7 Click reaction

Materials

Black 96-well Screenstar plates (Product number #655866, Greiner Bio-One, Frickenhausen, Germany) were used for immunostaining; copper sulfate, sodium ascorbate, Triton X-100, tris(3-hydroxypropyl-triazolylmethyl)amine (THPTA), phosphate buffered saline (PBS), and bovine serum albumin (BSA) were purchased from Sigma Aldrich; paraformaldehyde (PFA 16%) from Alfa Aesar; and Alexa Fluor™ 488 Azide (A10266) and Alkyne (A10267) from Invitrogen (Thermo Fisher Scientific). Azidoplatin was kindly provided by the DeRose lab.

Cell culture, treatment, and click reaction

Cells were cultured as described in Appendix I. A549 cells were seeded at t = 0 h in 96-well plates at a density of 5000 cells/well (100 μL) in OptiMEM complete and incubated for 24 h at 37 °C and 7.0% CO_2. At t = 24 h, the cells were treated with aliquots (100 μL) of either [**2**]Cl_2 (50 μM), [**4**]$(PF_6)_2$ (50 μM), or Azidoplatin (10 μM) and incubated for another 24 h. At t = 48 h, the plate was irradiated under air atmosphere using the cell-irradiation system (520 nm, 1 h, 76 J/cm^2) and further incubated. At t = 72 h, 24 h after irradiation, the wells were washed twice with 1X PBS (200 μL) and fixed with 4% PFA in PBS (100 μL) for 20 min under gentle shaking. Then, PFA was aspirated and 0.5% Triton X-100 in PBS (100 μL) was added and shacked for 20 min. After aspiration, the wells were washed twice with 3% BSA in PBS (100 μL) for 10 min while shaking. Hereafter, the 3% BSA solution was removed and the click cocktail in PBS was added (33 μL of 3 mM $CuSO_4$ in 15 mM THPTA or 33 μL of only 15 mM THPTA for Cu-free controls, 33 μL of 15 μM Alexa Fluor™ 488 (azide or alkyne, depending on tested compound), and 33 μL of 83 mM sodium ascorbate). The click mixture was shacked at room temperature for 1 h. Hereafter, the mixture was aspirated, and the wells were washed with 3% BSA in PBS, PBS, 0.5% Triton X-100, and finally PBS.

4.4.8 Imaging

Materials

Tween was purchased from Sigma Aldrich. PBST is 0.1% Tween in PBS. LAMP1 was purchased from Abcam (ab25245), Cy5 Goat Anti-Rat from Molecular Probes (Life Technologies Europe BV, Bleiswijk, The Netherlands). Anti-Giantin from Abcam (ab37266), Alexa Fluor™ 647 AffiniPure Goat Anti-Mouse IgG (H+L) from Jackson ImmunoResearch (115-605-146), NucBlue™ from Invitrogen (R37605).

Co-staining

The co-staining was performed in dim light. Wells were washed twice with 1% BSA in PBST for 10 min while gently shaking. For lysosome co-staining, the primary antibody (LAMP1 1:100 in PBST, 100 μL) was added and incubated for 1 h at r.t. After washing the wells three times with PBST (100 μL) for 5 min at r.t while shaking, the secondary antibody (Cy5 Goat Anti-Rat, 1:1000, 100 μL) was incubated for 1 h at r.t. For Golgi co-staining, the primary antibody (Anti-Giantin 1:500 in PBST, 100 μL) was added and incubated overnight at 4 °C. The wells were washed three times with PBST (100 μL) for 5 min at r.t while shaking. After aspiration, the secondary antibody (Alexa Fluor® 647 AffiniPure Goat Anti-Mouse IgG (H+L), 1:1500, 100 μL) was incubated for 1 h at r.t while shaking. After every co-staining, the wells were washed three times with PBST (100 μL) for 5 min at r.t while shaking. After aspiration, nuclear co-staining (NucBlue™, 1 drop/2 mL, 100 μL) was added and incubated for 1 h at r.t while shaking. Finally, the co-staining was aspirated, and the wells were filled with PBS (100 μL) for imaging.

Microscopy imaging

Inverted epifluorescence microscopy imaging was performed on a Leica fluorescent microscope (model DMi8) with Leica LAS X acquisition software using the 63x oil immersion objective. Modular excitation/emission filter cubes were used: DAPI (405 nm) for Hoechst 33342 (ex./em. 360/460 nm), GFP (470/40 nm) for Alexa Fluor™ 488 (ex./em. 495/519 nm), and Y5 (620/60 nm) for Alexa Fluor™ 647 (ex./em. 651/667 nm). Confocal imaging was performed on an Eclipse Ti2-C2+ Nikon confocal microscope using the 20x air objective (0.75 NA and 1.00 WD). Lasers used: 405 nm for Hoechst 33342 (ex./em. 360/460 nm), 488 nm for [**2**]$^{2+}$ and [**4**]$^{2+}$ labeled with Alexa Fluor™ 488 (ex./em. 495/519 nm), and 640 nm for Alexa Fluor™ 647 (ex./em. 651/667 nm). The settings for image acquisition (laser power and PMT gain) were identical for all conditions.

Fiji ImageJ software was used to process the images. The settings during image processing were identical for each condition. Hoechst, AlexaFluor488, and Anti-Giantin 647 were shown in blue, green, and red, respectively.

4.4.9 Supporting Information

The synthetic route for the synthesis of [**2**]$(PF_6)_2$ and [**4**]$(PF_6)_2$, ^{1}H NMR spectra of [**2**]$(PF_6)_2$ and [**4**]$(PF_6)_2$, geometry data of the DFT models, the molar extinction coefficients, singlet oxygen production and phosphorescence spectra, UV-vis and MS spectra of the green light activation, photosubstitution conditions for the calculations of the photosubstitution quantum yield by Glotaran, UV-vis spectra of the dark stability in water and cell medium, the light dose determination for [**2**]Cl_2 and [**4**]$(PF_6)_2$, as well as microscopy images of A549 cells treated with [**2**]Cl_2 and [**4**]$(PF_6)_2$ are provided in Appendix IV.

4.5 Contribution

Dr. Sylvia Le Dévédec performed confocal microscopy, Ingrid Flashpohler helped performing cytotoxicity tests, Dr. Claudia Schmidt and Prof. Ingo Ott performed HRCS-AAS measurements for cell uptake, Xuequan Zhou performed singlet oxygen measurements, Dr. Vincent van Rixel grew single crystals, and Dr. Maxime Siegler performed X-ray diffraction experiments and crystal structure determination. Dr. Sylvestre Bonnet performed DFT calculations and together with Prof. Lies Bouwman, he provided experimental guidance and significant editorial feedback.

4.6 References

1 H. U. Holtkamp and C. G. Hartinger, *Trends Anal. Chem.* **2018**, 104 (-), 110-117.

2 L. Zeng, Y. Chen, H. Huang, J. Wang, D. Zhao, L. Ji, and H. Chao, *Chem. Eur. J.* **2015**, 21 (43), 15308-15319.

3 R. A. Alderden, H. R. Mellor, S. Modok, T. W. Hambley, and R. Callaghan, *Biochem. Pharmacol.* **2006**, 71 (8), 1136-1145.

4 C. Molenaar, J.-M. Teuben, R. J. Heetebrij, H. J. Tanke, and J. Reedijk, *J. Biol. Inorg. Chem.* **2000**, 5 (5), 655-665.

5 K. Katano, R. Safaei, G. Samimi, A. Holzer, M. Tomioka, M. Goodman, and S. B. Howell, *Clinical Cancer Research* **2004**, 10 (13), 4578-4588.

6 R. Safaei, K. Katano, B. J. Larson, G. Samimi, A. K. Holzer, W. Naerdemann, M. Tomioka, M. Goodman, and S. B. Howell, *Clinical Cancer Research* **2005**, 11 (2), 756-767.

7 R. Safaei, B. J. Larson, T. C. Cheng, M. A. Gibson, S. Otani, W. Naerdemann, and S. B. Howell, *Mol. Cancer Ther.* **2005**, 4 (10), 1595-1604.

8 A. A. Nazarov, J. Risse, W. H. Ang, F. Schmitt, O. Zava, A. Ruggi, M. Groessl, R. Scopelitti, L. Juillerat-Jeanneret, C. G. Hartinger, and P. J. Dyson, *Inorg. Chem.* **2012**, 51 (6), 3633-3639.

9 A. Bahreman, J.-A. Cuello-Garibo, and S. Bonnet, *Dalton Trans.* **2014**, 43 (11), 4494-4505.

10 M. D. Hall, M. Okabe, D.-W. Shen, X.-J. Liang, and M. M. Gottesman, *Annu. Rev. Pharmacol. Toxicol.* **2008**, 48 (1), 495-535.

11 S. Ding, X. Qiao, J. Suryadi, G. S. Marrs, G. L. Kucera, and U. Bierbach, *Angew. Chem.* **2013**, 125 (12), 3434-3438.

12 R. Wirth, J. D. White, A. D. Moghaddam, A. L. Ginzburg, L. N. Zakharov, M. M. Haley, and V. J. DeRose, *J. Am. Chem. Soc.* **2015**, 137 (48), 15169-15175.

13 D. Hu, Y. Liu, Y.-T. Lai, K.-C. Tong, Y.-M. Fung, C.-N. Lok, and C.-M. Che, *Angew. Chem., Int. Ed.* **2016**, 55 (4), 1387-1391.

14 S. K. Fung, T. Zou, B. Cao, P.-Y. Lee, Y. M. E. Fung, D. Hu, C.-N. Lok, and C.-M. Che, *Angew. Chem.* **2017**, 129 (14), 3950-3954.

15 J. B. Gerken, M. L. Rigsby, R. E. Ruther, R. J. Pérez-Rodríguez, I. A. Guzei, R. J. Hamers, and S. S. Stahl, *Inorg. Chem.* **2013**, 52 (6), 2796-2798.

16 A. J. Göttle, F. Alary, M. Boggio-Pasqua, I. M. Dixon, J.-L. Heully, A. Bahreman, S. H. C. Askes, and S. Bonnet, *Inorg. Chem.* **2016**, 55 (9), 4448-4456.

17 C. Hansch, A. Leo, and R. Taft, *Chem. Rev.* **1991**, 91 (2), 165-195.

18 R. E. Goldbach, I. Rodriguez-Garcia, J. H. van Lenthe, M. A. Siegler, and S. Bonnet, *Chem.Eur. J.* **2011**, 17 (36), 9924-9929.

19 B. Siewert, M. Langerman, Y. Hontani, J. T. M. Kennis, V. H. S. van Rixel, B. Limburg, M. A. Siegler, V. Talens Saez, R. E. Kieltyka, and S. Bonnet, *Chem. Commun.* **2017**, 53 (81), 11126-11129.

20 L. N. Lameijer, T. G. Brevé, V. H. S. van Rixel, S. H. C. Askes, M. A. Siegler, and S. Bonnet, *Chem. Eur. J.* **2018**, 24 (11), 2709-2717.

21 J. Snellenburg, J., S. Laptenok, R. Seger, K. Mullen, M., and I. Van Stokkum, H.M., *J. Stat. Softw.* **2012**, 49 (3), 1-22.

22 S. Hopkins, B. Siewert, S. Askes, P. Veldhuizen, R. Zwier, M. Heger, and S. Bonnet, *Photochem. Photobiol. Sci.* **2016**, 15 (5), 644-653.

23 F. Wang, J. Bella, J. A. Parkinson, and P. J. Sadler, *J. Biol. Inorg. Chem.* **2005**, 10 (2), 147-155.

24 C. Mari, V. Pierroz, R. Rubbiani, M. Patra, J. Hess, B. Spingler, L. Oehninger, J. Schur, I. Ott, L. Salassa, S. Ferrari, and G. Gasser, *Chem. Eur. J.* **2014**, 20 (44), 14421-14436.

25 L. N. Lameijer, S. L. Hopkins, T. G. Brevé, S. H. C. Askes, and S. Bonnet, *Chem. Eur. J.* **2016**, 22 (51), 18484-18491.

26 F. E. Poynton, S. A. Bright, S. Blasco, D. C. Williams, J. M. Kelly, and T. Gunnlaugsson, *Chem. Soc. Rev.* **2017**, 46 (24), 7706-7756.

27 A. Ellinger and M. Pavelka, *Cell Tissue Res.* **1984**, 235 (1), 187-194.

28 V. Fernández-Moreira, F. L. Thorp-Greenwood, and M. P. Coogan, *Chem. Commun.* **2010**, 46 (2), 186-202.

29 K. K.-W. Lo, T. K.-M. Lee, J. S.-Y. Lau, W.-L. Poon, and S.-H. Cheng, *Inorg. Chem.* **2008**, 47 (1), 200-208.

30 K. K.-W. Lo, M.-W. Louie, K.-S. Sze, and J. S.-Y. Lau, *Inorg. Chem.* **2008**, 47 (2), 602-611.

31 C. L. Ho, K. L. Wong, H. K. Kong, Y. M. Ho, C. T. L. Chan, W. M. Kwok, K. S. Y. Leung, H. L. Tam, M. H. W. Lam, X. F. Ren, A. M. Ren, J. K. Feng, and W. Y. Wong, *Chem. Commun.* **2012**, 48 (19), 2525-2527.

32 X.-J. Liang, D.-W. Shen, K. G. Chen, S. M. Wincovitch, S. H. Garfield, and M. M. Gottesman, *J. Cell. Physiol.* **2005**, 202 (3), 635-641.

33 M. V. Babak, S. M. Meier, K. V. M. Huber, J. Reynisson, A. A. Legin, M. A. Jakupec, A. Roller, A. Stukalov, M. Gridling, K. L. Bennett, J. Colinge, W. Berger, P. J. Dyson, G. Superti-Furga, B. K. Keppler, and C. G. Hartinger, *Chem. Sci.* **2015**, 6 (4), 2449-2456.

34 S. M. Meier, D. Kreutz, L. Winter, M. H. M. Klose, K. Cseh, T. Weiss, A. Bileck, B. Alte, J. C. Mader, S. Jana, A. Chatterjee, A. Bhattacharyya, M. Hejl, M. A. Jakupec, P. Heffeter, W. Berger, C. G. Hartinger, B. K. Keppler, G. Wiche, and C. Gerner, *Angew. Chem., Int. Ed.* **2017**, 56 (28), 8267-8271.

35 R. M. Cunningham and V. J. DeRose, *ACS Chem. Biol*. **2017**, 12 (11), 2737-2745.

36 T. Funayama, M. Kato, H. Kosugi, M. Yagi, J. Higuchi, and S. Yamauchi, *Bull. Chem. Soc. Jpn.* **2000**, 73 (7), 1541-1550.

37 G. te Velde, F. M. Bickelhaupt, E. J. Baerends, C. Fonseca Guerra, S. J. A. van Gisbergen, J. G. Snijders, and T. Ziegler, *J. Comput. Chem.* **2001**, 22 (9), 931-967.